# Measurements of ground-state properties for nuclear structure studies by precision mass and laser spectroscopy

**K Blaum[1,2], M Block[3], RB Cakirli[1,4], S Eliseev[1], M Kowalska[1], S Kreim[1], YA Litvinov[1,3], Sz Nagy[1,3], W Nörtershäuser[3,5] and DT Yordanov[6]**

[1] Max-Planck-Institut für Kernphysik, 69117 Heidelberg, Germany
[2] Physikalisches Institut, Ruprecht-Karls-Universität Heidelberg, 69120 Heidelberg, Germany
[3] GSI Helmholtzzentrum für Schwerionenforschung, 64291 Darmstadt, Germany
[4] Department of Physics, University of Istanbul, Istanbul, Turkey
[5] Institut für Kernchemie, Johannes Gutenberg-Universität Mainz, 55128 Mainz, Germany
[6] CERN, Physics Department, 1211 Geneva 23, Switzerland

E-mail: klaus.blaum@mpi-hd.mpg.de

**Abstract.** Atomic physics techniques like Penning-trap and storage-ring mass spectrometry as well as laser spectroscopy have provided sensitive high-precision tools for detailed studies of nuclear ground-state properties far from the valley of $\beta$-stability. Mass, moment and nuclear charge radius measurements in long isotopic and isotonic chains have allowed extraction of nuclear structure information such as halos, shell and subshell closures, the onset of deformation, and the coexistence of nuclear shapes at nearly degenerate energies. This review covers experimental precision techniques to study nuclear ground-state properties and some of the most recent results for nuclear structure studies.

## 1. Introduction

Nuclear ground-state properties like masses, charge radii, spins and moments can be determined by applying atomic physics techniques such as Penning-trap and storage-ring based mass spectrometry and laser spectroscopy [1, 2, 3, 4]. In recent years, several breakthroughs in ion-beam cooling, manipulation and detection have been achieved giving, e.g., access to heavy nuclides with production yields of about 1 ion per 10 seconds and still reaching relative mass precisions below $10^{-7}$ [5]. Also new nuclides [6, 7] and isomers [8, 9] were discovered or unambiguously identified [10] by these techniques. The harvest in recent precision mass spectrometry experiments on short-lived nuclides is summarized in Fig. 1. This large amount of new high-precision data has allowed revealing new nuclear-structure phenomena and opening the door to new exciting nuclear physics discussions, which will be presented in this paper.

## 2. Experimental techniques

### *2.1. Penning-trap mass spectrometry*

At present, six Penning-trap based mass-spectrometry experiments are taking data at accelerators. These setups include in chronological order of the start of their data taking ISOLTRAP [11] at ISOLDE/CERN, the Canadian Penning trap (CPT) [12] at the Argonne National Laboratory ANL, the JYFLTRAP facility [13] in Jyväskylä, SHIPTRAP [14] at GSI/Darmstadt, LEBIT [15] at NSCL (MSU, East Lansing), and TITAN [16] at TRIUMF/Vancouver. TRIGA-TRAP [17] is the first Penning trap mass spectrometer at a nuclear research reactor and started taking off-line data at TRIGA-Mainz in 2009 [18]. One more accelerator-based setup is presently in the commissioning phase at MLL Munich [19].

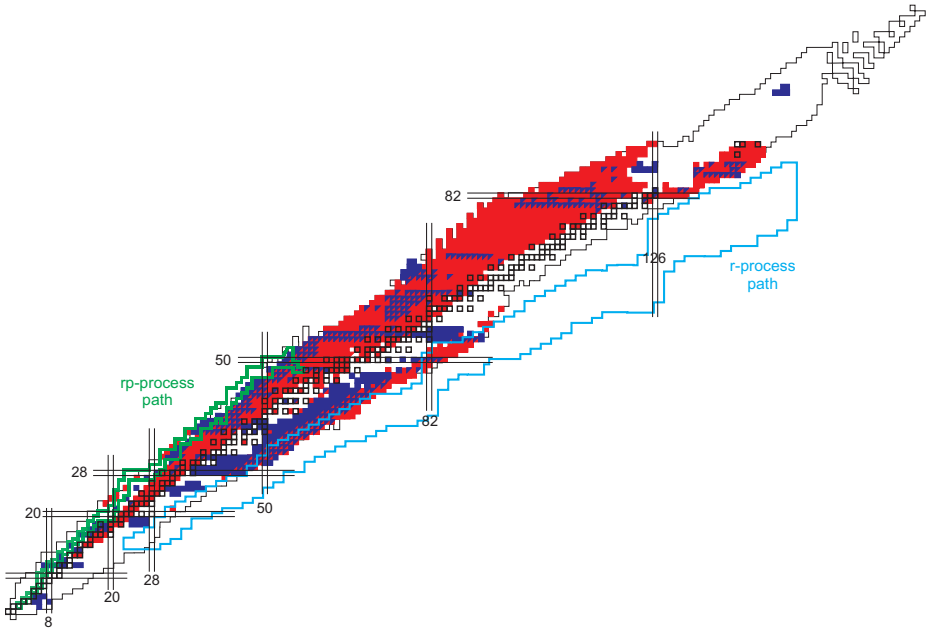


**Figure 1.** Color coded nuclear chart where stable nuclides are marked by black squares, all masses measured by storage-ring mass spectrometry are marked as red squares, those by Penning-trap mass spectrometry are marked as blue squares. Masses measured by both techniques are marked as triangles. The rp- and and r-process paths are shown on the neutron deficient and neutron rich side, respectively. Mass data until January 2010 have been considered here.

A Penning trap is operated using a strong homogeneous magnetic field of typically $B = 6$ to 9 T and a weak quadrupolar electrostatic trapping potential that is created by applying a voltage difference $U_0$ between the ring and endcap electrodes. The resulting eigenmotion of a stored charged particle is a superposition of three harmonic eigenmotions [20], however, only the cyclotron frequency $\nu_c = qB/(2\pi m)$ of an ion with charge-to-mass ratio $q/m$ is of interest here. To determine $\nu_c$ and thus the mass of the ion of interest, to date only the time-of-flight ion-cyclotron-resonance (TOF-ICR) detection technique is used for short-lived nuclides [21]. Here, ions are released from the trap and their flight time to a detector in the fringe field of the superconducting magnet is recorded. Prior to their ejection, ions are excited with an azimuthal quadrupolar RF field around $\nu_c$ either continuously [22] or with time-separated oscillatory fields [23, 24]. In case of a resonant excitation at $\nu_c$ the ion's radial kinetic energy is maximized, which is transformed into an additional axial acceleration while ions pass a magnetic field gradient. Atomic masses $m$ are derived using alternating calibration measurements of nuclides with precisely known mass values or close-by carbon cluster ions $^{12}C_n^+$ for absolute mass calibration [25, 26]. In this way, relative mass uncertainties $\delta m/m$ as low as a few times $10^{-9}$ are nowadays achieved. At TRIGA-TRAP, in addition to TOF-ICR, the non-destructive Fourier-transform ion-cyclotron-resonance (FT-ICR) detection technique is being developed, where the cyclotron frequency of the oscillating ion is measured via the induced image currents in the segmented ring electrode [27].

### *2.2. Storage ring mass spectrometry*

High-energy storage rings offer a possibility of simultaneous mass and, in many cases, half-life measurements of several ten nuclides in one experiment. There are two operational facilities, namely ESR at GSI in Darmstadt and CSRe at IMP in Lanzhou, which are coupled to high-energy synchrotrons SIS and CSRm via the in-flight fragment separators FRS and RIBLL2, respectively [28]. Exotic nuclei are produced at high energies employing fragmentation or, in case of uranium, fission of primary beam

particles. The reaction products are injected and stored at 300-400 MeV/u and the ions are produced with no or very few bound electrons. Due to the production mechanism, the ions inevitably have a momentum spread of a few percent, which can be reduced by stochastic and electron cooling. For the electron cooled ions, the revolution frequencies of the ions reflect their mass-over-charge ratios. In Schottky Mass Spectrometry (SMS), these frequencies are measured non-destructively by a dedicated pick-up detector [3]. The advantage of SMS is that a single stored ion is often sufficient to determine its mass to a relative mass uncertainty of about $\delta m/m \approx 2 \cdot 10^{-7}$ [29]. For instance, five new nuclides ($^{213}$Tl, $^{221,222}$Po, $^{224}$At and $^{236}$Ac) were thus recently discovered and their half-lives and masses measured [7]. In special cases, by limiting the analyzed frequency bandwidth, mass uncertainties of a few $10^{-8}$ can be achieved [30]. The cooling, however, takes a few seconds, which limits the number of accessible nuclei due to their half-lives.

In order to address shorter lived nuclides, an isochronous ion-optical setting of the ring is applied, in which the momentum spread of the ions is (in first order) compensated by the orbit lengths of the circulating ions [31] and no cooling is required. The frequencies are obtained from a dedicated detector which contains a few $\mu$g/cm$^2$ thick carbon foil and acquires signals from each particle passing through the detector at each revolution in the ring. This method is called Isochronous Mass Spectrometry (IMS). Typically, ions are stored for a few hundred revolutions before they are lost from the ring acceptance mainly due to energy loss in the detector foil. The frequencies are typically about 2 MHz, thus, the method allows studying nuclei with half-lives down to a few ten $\mu$s, as demonstrated for the 4.56(10) MeV isomeric state in $^{133}$Sb (see [32] for more details).

Although the mass uncertainty of $\delta m/m \approx 10^{-6} - 10^{-7}$ achieved in storage-ring experiments is somewhat lower than the one achieved in Penning-trap measurements, they can address exotic isotopes with very-low production rates of one ion per day or even per week. We note that a new resonant Schottky pick-up is being presently commissioned at the ESR, which enables frequency measurements of single ions within a few ten milliseconds [33].

### *2.3. Collinear laser spectroscopy*

Collinear laser spectroscopy is one of the most prominent techniques ever established for studying spins, electromagnetic moments and root mean square (rms) charge radii of exotic atoms. These constitute highly sensitive probes of the nuclear single-particle and collective structure, which are of great importance for theoretical modeling of the atomic nucleus. Even though it has been in use for more than three decades, collinear laser spectroscopy is still at the frontier of experimental nuclear physics due to important improvements, which provide increased sensitivity and outstanding precision needed to fulfill the demands associated with the most recent challenges in nuclear physics.

*2.3.1. Classical fluorescence spectroscopy* The basis of collinear laser spectroscopy by fluorescence detection is the overlapping of a fixed-frequency laser beam with a beam of ions accelerated to a few ten keV. This collinear method results in a low velocity spread and electron transition line widths close to the natural width, given by the atomic-transition lifetime in the uncertainty principle. In order to find atomic transitions, the ion-beam velocity is varied by post acceleration changing the Doppler shift. At a discrete spectrum of velocities (Doppler-shifted laser frequencies) laser radiation is absorbed by the particle beam followed by spontaneous fluorescence, which is monitored. One limitation for the efficiency of this method is the usually small solid angle that can be covered with photo detection. In order to reach higher sensitivity, the detection of charged particles instead of photons, such as detection of $\beta$-particles from laser-oriented nuclei [34], collisional ionization [35], radioactivity detection after state-selective charge exchange [36], or collinear laser ionization [37], was applied in many cases.

In order to reduce the background the concept of collinear laser spectroscopy on bunched beams has been developed in 2002 at the IGISOL facility [38] and recently also implemented at ISOLDE [39]. The beams are accumulated in a radio-frequency quadrupole (RFQ) and then released in short bunches. The accumulation time $T_1$ is chosen short enough to avoid overfilling of the trap and decay losses. The bunch

width $T_2$ is defined by the RFQ. By gating the fluorescence detection on the bunched beam structure one can reduce the background from laser scattering and dark noise of the photo tubes by a factor of typically $T_2/T_1 = 10000$, and improve the signal-to-noise ratio with its square root. Typical time constants are $T_1 = 100$ ms and $T_2 = 10\,\mu s$. As a result, this method can cope with a yield of a few 100 ions/s and thus about two orders of magnitude lower yields than classical fluorescence spectroscopy, as long as it is not hampered by vast yields of isobars that will quickly overfill the ion trap.

*2.3.2. Collinear-anticollinear method with a frequency comb for ultimate precision* In light nuclei, the volume effect is a small fraction of the measured isotope shift, typically on a level comparable with the systematic uncertainties of the laser frequency and the ion-beam energy. In order to extract accurate radii the latter has to be known precisely. A direct measurement of the voltage used for particle acceleration is practically impossible to the required precision. Laser frequencies, on the other hand, can be locked to precisely known atomic transitions, for instance of iodine, or be directly linked to an RF frequency standard via a frequency comb. The essence of the method is to apply two laser beams, collinear $\nu_c$ and anticollinear $\nu_a$ with respect to the ion beam. If one of the lasers is locked to a frequency comb, it versatiles such measurements because its frequency can be adjusted to the point where resonances are observed from both lasers at approximately the same post-acceleration voltage. Consequently, the acceleration voltage and the absolute transition frequency $\nu_0$ can be determined precisely using the relation $\nu_c \cdot \nu_a = \nu_0^2$ [40, 41].

## 3. Nuclear structure studies

### *3.1. Nuclear halos*

In neutron-halo nuclei two effects contribute to the size of the proton distribution inside the nucleus: halo neutrons cause the core nucleus to move around the center of mass (CM) of the composite system. Hence, a larger effect is expected for a one-neutron halo nucleus, whereas in a two- or four-neutron halo the size of this effect strongly depends on the correlation between the halo neutrons. On the other hand, the neutron(s) in the halo interact(s) with the core nucleus and might give rise to core polarization and, hence, change the proton distribution. Information from different experiments have to be combined to disentangle these effects. Nuclear charge radii obtained from isotope-shift measurements provide accurate and reliable data about the nuclear size, since it can be extracted in a nuclear-model independent way, which has been demonstrated for lithium [42, 43] and helium isotopes [44, 45]. Such measurements became possible because new atomic physics calculations including quantum-electrodynamics and relativistic effects reached an accuracy of a few times $10^{-6}$ for three-electron systems [46] for the prediction of the mass-dependent isotope shift, and similarly accurate isotope shift measurements are available. This allowed for the first time the separation of the nuclear volume contribution in very light exotic nuclei, which accounts for only a $10^{-5}$ fraction of the total isotope shift. In addition the masses of the halo nuclides of interest have to be known with a relative precision of the order of $10^{-7}$ or better for sufficiently accurate calculation of the mass shift. Therefore recent mass measurements that were reported for the neutron halo nuclides $^{6,8}$He [47, 48], $^{11}$Li [49, 50], $^{11,12}$Be [51, 52], and the two-proton halo candidate $^{17}$Ne [53], provided important input data for these calculations and increased the accuracy of the charge radii results.

Even though the mass-shift calculations were steadily improved in recent years [54, 55], still today they reach the required accuracy only for three-electron systems. The first measurement of the charge radius of a one-neutron halo nucleus was recently reported on $^{11}$Be [40]. Here, collinear-anticollinear laser spectroscopy as described above was performed and absolute transition frequencies were measured with relative accuracy of about $10^{-9}$. The nuclear charge radii of $^{7,10,11}$Be were determined based on the elastic electron scattering result for the charge radius of the stable isotope $^{9}$Be [56]. The results are in very good agreement with fermionic molecular dynamics (FDM) calculations along the investigated isotopic chain, as can be seen in Fig. 2. If the change in charge radius between $^{10}$Be and the one-neutron halo nucleus $^{11}$Be is solely ascribed to the geometric effect of center-of-mass motion, the halo neutron

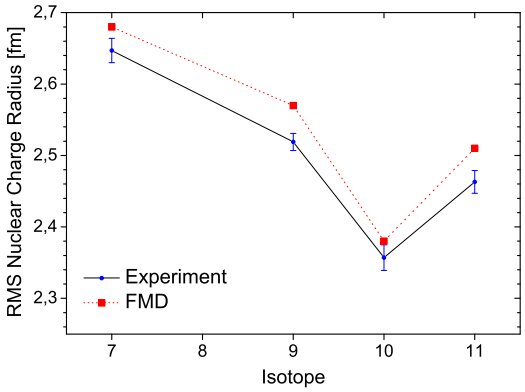


**Figure 2.** Experimental charge radii of beryllium isotopes from isotope-shift measurements (dots) compared with values from fermionic molecular dynamics calculations (squares). Based on [41].

must be at a distance of about 7 fm from the CM. Comparisons with the FMD calculations and results from nuclear breakup reactions [57] indicate that there is probably a small contribution of nuclear core polarization [41]. Further measurements on $^{12}$Be are planned to be performed at ISOLDE in 2010.

The effect of halo-neutron correlation can be readily observed in the helium isotopes. Here, the core is a strongly bound alpha particle and core polarization is therefore expected to be very weak. The four-neutron halo isotope $^{8}$He has a significantly smaller charge radius than the two-neutron halo isotope $^{6}$He, due to a distribution of the additional neutrons shifting the CM closer to the core. However, in $^{11}$Li core polarization of the much softer $^{9}$Li core cannot be assumed to be comparably small from the beginning [58, 59], hence, additional data from other sources must be used to obtain a conclusive picture of this halo nucleus.

### *3.2. Shell and subshell closures in neutron-rich nuclides*

The nuclear binding energy reflects all interactions acting between the nucleons inside the atomic nucleus. By applying the proper filters, one can isolate specific parts of the interaction. In this way shell and subshell closures can be very well brought to light by following the changes in the binding energy when adding neutrons or protons. The most commonly used filter is the neutron or proton separation energy, i.e. the energy required to remove the last neutron (proton), defined as the difference in binding energy $B(N, Z)$ for neighboring nuclei. In order to avoid pairing effects leading to an odd-even staggering in binding energies $B$, one plots in practice two-neutron (two-proton) separation energies, defined as follows:

$$S_{2n} = B(N-2, Z) - B(N, Z), \quad S_{2p} = B(N, Z-2) - B(N, Z). \tag{1}$$

Generally, $S_{2n}$ ($S_{2p}$) decreases smoothly with neutron (proton) number. Shell effects appear as a sudden drop at closed shells, where the nucleons start filling a new shell. For a more quantitative information one can study the two-nucleon gaps, i.e. the first derivatives of separation energies

$$\Delta_{2n} = S_{2n}(N, Z) - S_{2n}(N+2, Z), \quad \Delta_{2p} = S_{2p}(N, Z) - S_{2p}(N, Z+2), \tag{2}$$

which are approximately equal to twice the gap in the single-particle orbits. It should be kept in mind that the observed $\Delta_{2n}$ and $\Delta_{2p}$ are "effective" shell gaps, since next to the single-particle shell gap they also include effects due to the residual interaction between valence nucleons, mostly monopole, pairing and quadrupole correlations. These many-body effects can lead to a decrease of the "effective" shell gap or can even smear out the shell-gap effect altogether while the underlying single-particle gap does not necessarily change [60, 61].

Recent mass measurements addressed several shell and subshell closures for both neutrons and protons. The As the neutron dripline is approached evolution of the $N = 28$ shell closure has been studied for $^{36-42}$Si, $^{40-44}$P, $^{43-45}$S, and $^{43,45-47}$Cl with the time-of-flight technique using the SPEG spectrometer [62]. Changes in shell structure were observed for P and S isotopes but not for Si. The observed trend may be interpreted as a persistence of the shell closure or as the result of a very sudden onset in deformation at $^{42}$Si. The LEBIT mass spectrometer has also probed the $N = 28$ shell closure based on improved masses of neutron-rich $^{40-44}$S isotopes [63]. The resulting trend in $S_{2n}$ for S as it crosses $N = 28$ remains undetermined due to the large uncertainty in the SPEG mass value of $^{45}$S.

The ISOLTRAP experiment has provided over 30 masses around $Z = 28$ and $N = 40$, namely $^{57,60,64-69}$Ni ($Z = 28$), $^{65-74,76}$Cu ($Z = 29$), and $^{63-65,68-78}$Ga ($Z = 31$) [64]. While the classic indications from the $S_{2n}$ values showed no strong evidence for a shell closure at $N = 40$, there was evidence for a weak and very localized effect for $Z = 28$, consistent with findings from nuclear spectroscopy studies. Masses of $^{70-73}$Ni and $^{73,75}$Cu studied at JYFLTRAP gave a slope change in nickel $S_{2n}$ values beyond $N = 40$ and a slight increase in $\Delta_{2n}$ at $N = 40$ for $Z = 28$ [65], similar to the ISOLTRAP results. $S_{2p}$ values, on the other hand, show a pronounced shell effect at $Z = 28$. In addition, the trend in both neutron and proton separation energies agrees with the predictions based on the effect of the tensor interaction. The $N = 40$ subshell closure was more recently addressed also at the LEBIT setup with the masses of $^{63-66}$Fe and $^{64-67}$Co [66]. Unfortunately, the observed small discontinuities in the $S_{2n}$ values reported previously in neighboring chains of Ni, Cu, and Ga isotopes could not be confirmed in the Co isotopes due to the large error bars above $N = 40$.

The evolution of the $N = 50$ shell gap energy towards the doubly-magic $^{78}$Ni has been investigated using IMS at the FRS-ESR. The mass measurements of $^{79-80}$Ga, $^{82-83}$Ge, $^{83-86}$As, and $^{86-89}$Se [67] showed a decreasing trend of "effective" shell gap energies down to $Z = 33$. Studies in the same region have been extended at JYFLTRAP to more neutron-rich nuclides $^{76-80}$Zn, $^{78-83}$Ga, $^{80-85}$Ge, $^{81-87}$As, and $^{84-89}$Se, ten of which were not known before [68]. The obtained $S_{2n}$ values confirm the reduction of the $N = 50$ "effective" shell gap energy towards $Z = 32$ and show a subsequent increase at $Z = 31$, which corresponds to a minimum in the measured first $2^+$ energies of $N = 50$ isotones. The $S_{2n}$ trend indicates as well that the gap at $N = 50$ opens up when moving further towards $^{78}$Ni at $Z = 28$. The best agreement with theory is observed for the finite-range liquid drop model [69] and the projected GCM method with Skyrme interaction [70]. The latter, however, predicts a further decrease in the "effective" shell gap at $^{78}$Ni connected to a gradual decrease in the underlying spherical shell gap and increase in quadrupole correlations. In the same region, ISOLTRAP studies of neutron-rich Zn isotopes included the mass of $^{80}$Zn which agrees with the JYFLTRAP result, as well as that of $^{81}$Zn which was determined experimentally for the first time [71]. Based on the improved mass extrapolation of $^{82}$Zn, the resulting $S_{2n}$ values and their comparison with several models showed the robustness of the $N = 50$ shell closure for $Z = 30$. This agrees with the shell gap trend observed down to $Z = 31$ at JYFLTRAP. For a summary of the above results see Fig. 3.

In the $Z = 50$, $N = 82$ region, ISOLTRAP has revealed a 0.5-MeV deviation of the binding energy of $^{134}$Sn [72] from the previously accepted value [73], which restored the neutron-shell gap at $N = 82$, previously considered to be a case of "shell quenching". This finding has been recently confirmed by the single-particle nature of excited states in $^{133}$Sn [74], with just one neutron outside the $N = 82$ core. In addition, the resulting "effective" shell gap for $^{132}$Sn turned out to be larger than that of the stable doubly-magic $^{48}$Ca. More high-precision mass data in the region of $N = 82$ up to $N = 100$ have been obtained recently at CPT [75], which is an extension of the work reported in [12].

### *3.3. Proton-neutron interaction*

Double differences of binding energies, $\delta V_{pn}$, given for even-even nuclei in Eq. 3, are a special filter to cancel out all the interactions except the interactions between the last protons and the last neutrons. In the first two binding energies, the $N$ and $(N-1)$ neutrons interact with $Z$ protons, each other and with all the other $(N-2)$ neutrons. In the third and the fourth binding energies, $N$ and $(N-1)$ neutrons will

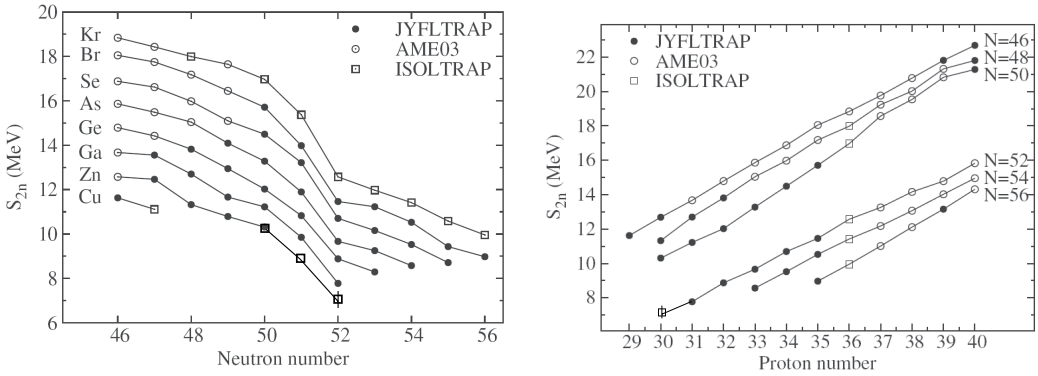


**Figure 3.** Left: The two-neutron separation energies as a function of neutron number for neutron-rich nuclides around $N = 50$. Experimental values from AME2003, JYFLTRAP, and ISOLTRAP are shown. The $S_{2n}$ value of $^{82}$Zn is based on an extrapolation of its mass. Right: The same as left but as a function of proton number. Based on [68].

interact with $(Z-2)$ protons, each other and with all the other $(N-2)$ neutrons. Taking differences of these interactions will leave over an interaction of $N$ and $(N-1)$ neutrons with $Z$ and $(Z-1)$ protons. Note that if this filter cancels out changes in structure to second order. For example, if the structure changes with $N$, $\delta V_{pn}$ will still give the p-n interaction as long as the change with $N$ is similar in the isotopes of element $Z$ and $(Z-2)$.

$$\delta V_{pn}(Z,N) = \frac{1}{4}[(B(Z,N) - B(Z,N-2)) - (B(Z-2,N) - B(Z-2,N-2))] \quad (3)$$

Shell-model orbits can be used to understand this interaction in terms of the spatial overlap between the outermost nucleons of a given nucleus. Within a major shell, orbits with high angular momentum $j$ and low principal quantum number $n$ occur at the beginning of a shell while the same shell ends with low $j$ and high $n$ orbits (ignoring unique parity orbits). If protons and neutrons are filling similar orbits (similar $nl_j$), we expect large $\delta V_{pn}$ values because the overlap of similar orbits leads to large p-n interactions. If not, a low $\delta V_{pn}$ value is expected. The best example is the nucleus $^{208}$Pb where the $Z = 82$, $N = 126$ shells are completely filled so that the last particles of each type are at the end of their respective shells and have similar $nl_j$ resulting in a large $\delta V_{pn}$ value [76] (see Fig. 4). Adding two additional neutrons ($N = 128$, $^{210}$Pb), we expect low $\delta V_{pn}$ values. For $\delta V_{pn}$($^{210}$Pb)), the only missing mass of $^{208}$Hg has been measured with SMS in the ESR from a single stored hydrogen-like ion [77], yielding the first empirical $\delta V_{pn}$ for even neutron numbers beyond $N = 126$ with $Z \leq 82$ (see Fig. 4). Significant progress was made in heavy nuclei, where, for instance, a chain of radon isotopes has been investigated at ISOLTRAP [6]. The masses of $^{223-229}$Rn isotopes were obtained for the first time ($^{229}$Rn is the first isotope discovered by a Penning trap measurement).

Modern microscopic theories such as the Density Functional Theory (DFT) [78] can be used to calculate nuclear binding energies and the calculated $\delta V_{pn}$ values using those binding energies can be compared with the experimental ones. Figure 5 shows two $Z$ versus $N$ plots where the boxes are color coded with the empirical $\delta V_{pn}$ results (left) [76, 79] and the DFT results (right) [80]. These DFT results are based on a self-consistent solution of the Hartree-Fock-Bogoliubov equations with a mix-typed pairing and the SkP Skyrme force. The best agreement is expected in well-deformed nuclei since the existing DFT results succeed less well near closed shells and in regions of octupole deformation. As seen from Fig. 5, DFT agreement with data is impressive in general. The largest experimental $\delta V_{pn}$ values are in the particle-particle (p-p) region ($Z = 50 - 66$, $N = 82 - 104$, see Ref. [81] for more details) and the lowest $\delta V_{pn}$ values are in the hole-particle (h-p) region ($Z = 66 - 82$, $N = 82 - 104$). In addition, in terms of the fractional filling of the respective proton and neutron major shells, one expects

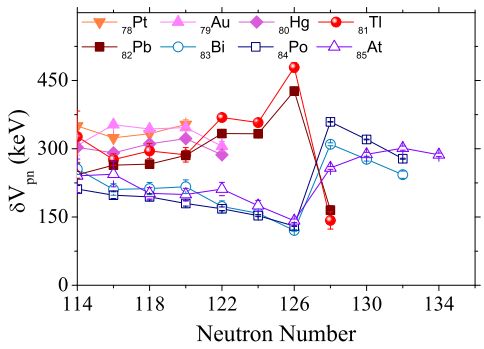


**Figure 4.** (Color online) Empirical $\delta V_{pn}$ values for the $^{208}$Pb region as a function of neutron number.

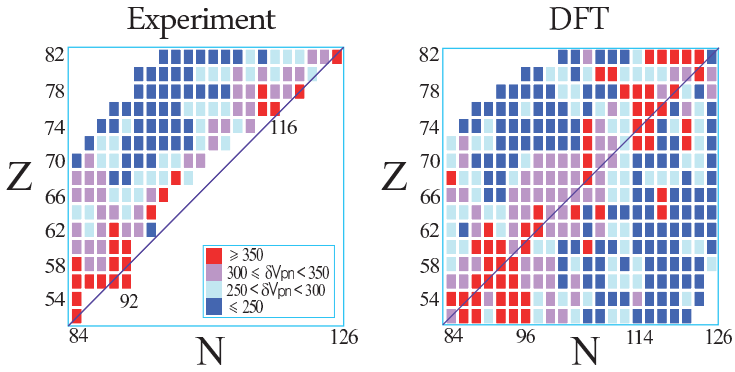


**Figure 5.** (Color online) The color coded $\delta V_{pn}$ values are illustrated for the $Z = 50 - 82$, $N = 82 - 126$ regions. $\delta V_{pn}$ is decreasing from red to dark blue [76, 79, 80]. Left: Experimental $\delta V_{pn}$ values. Right: Density Functional Theory results.

to see large $\delta V_{pn}$ values along the diagonal line in Fig. 5 [76, 81] and the DFT, again, agrees with this expectation nicely.

*3.4. Penning trap mass measurements on heavy and superheavy nuclides*

The region of the superheavy elements (SHE) ($Z > 103$) is of particular interest for nuclear structure physics since these elements owe their very existence entirely to nuclear shell effects. However, still today different theoretical models disagree in their prediction of the location of the "island of stability" inhabited by spherical SHE covering proton numbers $Z = 114$, 120 or 126 and neutron numbers $N = 172$ or 184 [82]. The experimental investigation of SHE is challenging as they are synthesized in fusion-evaporation reactions only with low production rates down to about one atom per week for cross sections on the picobarn level. Nonetheless, in the last decades the synthesis of superheavy elements up to copernicium has been achieved [83] and the latest claims reach even up to $Z = 118$ [84]. However, the latter elements produced in $^{48}$Ca induced reactions on actinide targets are still disconnected from the region of known nuclides and lack an unambiguous $Z$ and $A$ identification.

For a better understanding of superheavy elements detailed experimental studies by decay spectroscopy and direct mass measurements are crucial. Masses are of particular importance as they directly provide nuclear binding energies. Moreover, masses and derived quantities such as nucleon separation energies are input parameters for cross-section calculations and serve as a benchmark for different nuclear models. In addition, direct high-precision mass measurements provide reliable anchor points to fix $\alpha$-decay chains as recently demonstrated for three nobelium isotopes [85] whose masses have been measured with SHIPTRAP [5]. These nobelium isotopes are embedded into long $\alpha$-decay chains

and allow fixing the masses of heavier nuclides that are too short-lived to be accessed with Penning traps. A direct mass measurement is not prone to uncertainties introduced by missing excited states as they are often populated in the $\alpha$-decay of odd-odd or odd-$A$ nuclei.

The Penning-trap mass spectrometer SHIPTRAP [14] at GSI is presently the only one worldwide where masses of nuclides above fermium can be measured. It has been recently demonstrated that Penning trap mass measurements of heavy radionuclides with production rates of only about one ion per minute are presently feasible with SHIPTRAP. However, in order to access the heaviest elements that are only available in quantities of a few atoms a different detection technique as discussed in [86] has to be applied. Using an image current detection employing resonant tank circuits will then allow a mass determination based on the non-destructive detection of a single ion. The method can be applied to rare isotopes with half-lives longer than about 1 s, a condition fulfilled by several nuclides in the SHE region. This will also open up new possibilities for the $A/Q$ identification of new elements in the future.

## 4. Summary and Outlook

As demonstrated by the recent exciting results in nuclear structure studies achieved by high-precision mass- and laser-spectroscopic experiments, tremendous progress has been made in the last few years in these techniques. However, one major limiting factor in the investigation of nuclides far from stability is still the low yield of very neutron rich or neutron deficient nuclides. In order to get access to nuclides closer to the driplines new Penning-trap, storage-ring and laser-spectroscopy facilities are presently under construction, among them MATS and LaSpec [87] and ILIMA [88] at the FAIR facility.

## Acknowledgments

We acknowledge financial support by the Max-Planck Society, the Humboldt Foundation (R.B.C.) and the Helmholtz Association under contracts (Alliance Program: HA216/EMMI) and (VH-NG-148).

[1] Blaum K 2006 *Phys. Rep.* **425** 1
[2] Blaum K, Novikov YN and Werth G 2010 *Contemp. Phys.* **51** 149
[3] Franzke B, Geissel H and Münzenberg G 2008 *Mass Spectrom. Rev.* **27** 428
[4] Kluge HJ and Nörtershäuser W 2003 *Spectrochim Acta B* **58** 1031
[5] Block M et al. 2010 *Nature* **463** 785
[6] Neidherr D et al. 2009 *Phys. Rev. Lett.* **102**, 112501
[7] Chen L et al. 2010 *Phys. Lett. B* **691** 234
[8] Sun B et al. 2007 *Eur. Phys. J. A* **31** 393
[9] Block M et al. 2008 *Phys. Rev. Lett.***100** 132501
[10] Van Roosbroeck et al. 2004 *Phys. Rev. Lett.***92** 112501
[11] Mukherjee M et al. 2008 *Eur. Phys. J. A* **35** 1
[12] Savard G et al. 2006 *Int. J. Mass Spectrom.* **251** 252
[13] Kolhinen VS et al. 2004 *Nucl. Instrum. Meth. A* **528** 776
[14] Block M et al. 2007 *Eur. Phys. J. D* **45** 39
[15] Ringle R et al. 2006 *Int. J. Mass Spectrom.* **251** 300
[16] Dilling J et al. 2006 *Int. J. Mass Spectrom.* **251** 198
[17] Ketelaer J et al. 2008 *Nucl. Instrum. Meth. A* **594** 162
[18] Ketelaer J et al. 2010 *Eur. Phys. J. D* **58** 47
[19] Kolhinen VS et al. 2009 *Nucl. Instrum. Meth. A* **600** 391
[20] Brown LS and Gabrielse G 1986 *Rev. Mod. Phys.* **58** 233
[21] Gräff G, Kalinowsky H and Traut J 1980 *Z. Phys. A* **297** 35
[22] König M et al. 1995 *Int. J. Mass Spectrom. Ion process.* **142** 95
[23] Kretzschmar M 2007 *Int. J. Mass Spectrom.* **264** 122
[24] George S et al. 2007 *Int. J. Mass Spectrom.* **264** 110
[25] Blaum K et al. 2002 *Eur. Phys. J. A* **15** 245
[26] Kellerbauer A et al. 2003 *Eur. Phys. J. D* **22** 53
[27] Ketelaer J et al. 2009 *Eur. Phys. J. A* **42** 311
[28] Litvinov Yu A et al. 2010 *Acta Phys. Polonica B* **41** 511
[29] Litvinov Yu A et al. 2005 *Nucl. Phys. A* **756** 3

[30] Litvinov Yu A et al. 2006 *Hyp. Interactions* **173** 55
[31] Stadlmann J et al. 2004 *Phys. Lett. B* **586** 27
[32] Sun B et al. 2010 *Phys. Lett. B* **688** 294
[33] Nolden F et al. 2010 *in preparation*
[34] Arnold E et al. 1987 *Phys. Lett. B* **197** 311
[35] Neugart R et al. 1986 *Nucl. Instrum. Meth. B* **17** 354
[36] Vermeeren L et al. 1992 *Phys. Rev. Lett.* **68** 1679
[37] Schulz Ch et al. 1991 *J. Phys. B* **24** 4831
[38] Nieminen A et al. 2002 *Phys. Rev. Lett.* **88** 094801
[39] Mane E et al. 2009 *Eur. Phys. J. A* **42** 503
[40] Nörtershäuser W et al. 2009 *Phys. Rev. Lett.* **102** 062503
[41] Zakova M et al. 2010 *J. Phys. G* **37** 055107
[42] Ewald G et al. 2004 *Phys. Rev. Lett.* **93** 113002
[43] Sanchez R et al. 2006 *Phys. Rev. Lett.* **96** 033002
[44] Wang LB et al. 2004 *Phys. Rev. Lett.* **93** 142501
[45] Müller P et al. 2007 *Phys. Rev. Lett.* **99** 252501
[46] Yan ZC and Drake GWF 2000 *Phys. Rev. A* **61** 022504
[47] TITAN team, private communication (2010)
[48] Ryjkov VL et al. 2008 *Phys. Rev. Lett.* **101** 012501
[49] Bachelet C et al. 2008 *Phys. Rev. Lett.* **100** 182501
[50] Smith M et al. 2008 *Phys. Rev. Lett.* **101** 202501
[51] Ringle R et al. 2009 *Phys. Lett. B* **675** 170
[52] Ettenauer S et al. 2010 *Phys. Rev. C* **81** 024314
[53] Geithner W et al. 2008 *Phys. Rev. Lett.* **101** 252502
[54] Yan ZC, Nörtershäuser W and Drake GWK 2008 *Phys. Rev. Lett.* **100** 243002
[55] Puchalski M and Pachucki K 2008 *Phys. Rev. A* **78** 052511
[56] Jansen JA et al. 1972 *Nucl. Phys. A* **188** 337
[57] Palit R et al. 2003 *Phys. Rev. C* **68** 034318
[58] Borremans D et al. 2005 *Phys. Rev. C* **72** 044309
[59] Neugart R et al. 2008 *Phys. Rev. Lett.* **101** 132502
[60] Novikov Yu N et al. 2002 Nucl. Phys. A **697** 92
[61] Bender M, Bertsch GF and Heenen PH 2008 *Phys. Rev. C* **78** 054312
[62] Jurado B et al. 2007 *Phys. Lett. B* **649** 43
[63] Ringle R et al. 2009 *Phys. Rev. C* **80** 064321
[64] Guenaut C et al. 2007 *Phys. Rev. C* **75** 044303
[65] Rahaman S et al. 2007 *Eur. Phys. J. A* **34** 5
[66] Ferrer R et al. 2010 *Phys. Rev. C* **81** 044318
[67] Sun B et al. 2008 *Nucl. Phys. A* **812** 1
[68] Hakala J et al. 2008 *Phys. Rev. Lett.* **101** 052502
[69] Möller P et al. 1995 *At. Data Nucl. Data Tables* **59** 185
[70] Bender M, Bertsch GF and Heenen PH 2006 *Phys. Rev. C* **73** 034322
[71] Baruah S et al. 2008 *Phys. Rev. Lett.* **101** 262501
[72] Dworschak M et al. 2008 *Phys. Rev. Lett.* **100** 072501
[73] Audi G et al. 2003 *Nucl. Phys. A* **729** 3
[74] Jones KL et al. 2010 *Nature* **465** 454
[75] Van Schelt J et al. 2010 *to be published*
[76] Cakirli RB et al. 2005 *Phys. Rev. Lett.* **94** 092501
[77] Chen L et al. 2009 *Phys. Rev. Lett.* **102** 122503
[78] Stoitsov MV et al. 2006 *Int. J. Mass Spectrom.* **251**, 243
[79] Neidherr D et al. 2009 *Phys. Rev. C* **80**, 044323
[80] Stoitsov MV, private communication (2010)
[81] Cakirli RB and Casten RF 2006 *Phys. Rev. Lett.* **96** 132501
[82] Patyk Z and Sobiczewski A 1991 *Nucl. Phys. A* **533** 132; Bender M et al. 2003 *Rev. Mod. Phys.* **75** 121
[83] Hofmann S and Münzenberg G 2000 *Rev. Mod. Phys.* **72** 733
[84] Oganessian Yu 2007 *J. Phys. G* **34** R165
[85] Dworschak M et al. 2010 *Phys. Rev. C* **81** 064312
[86] Ketelaer J et al. 2009 *Eur. Phys. J. A* **42** 311
[87] Rodriguez D et al. 2010 *Eur. Phys. J. Spec. Topics* **183** 1
[88] Walker PM et al. 2005 *Technical proposal for the ILIMA project*, Report (GSI)